Journal of Sound and Vibration (1999) **222**(2), 281–305
Article No. jsvi.1998.2063, available online at http://www.idealibrary.com on IDEAL

DYNAMICS OF A SLENDER BEAM WITH AN ATTACHED MASS UNDER COMBINATION PARAMETRIC AND INTERNAL RESONANCES, PART II: PERIODIC AND CHAOTIC RESPONSES

S. K. DWIVEDY AND R. C. KAR
Department of Mechanical Engineering, Indian Institute of Technology, Kharagpur 721 302, *India*

(*Received* 15 *September* 1997, *and in final form* 29 *October* 1998)

The governing second order temporal differential equation of a slender beam with an attached mass at an arbitrary position under vertical base excitation which retains the cubic non-linearities of geometric and inertial type is reduced to a set of first order differential equations by the method of *normal forms* for combination parametric and internal resonances of 3:1. These equations are used to find the periodic, quasi-periodic and chaotic responses of the system for various bifurcating parameters, namely, damping, amplitude and frequency of base motion, attached mass and its location. Bifurcation set, mixed-mode oscillation, period-doubling, quasi-periodic orbits and different routes to chaos, namely, alternate periodic-chaotic transition, torus breakdown and intermittency have been studied for the above mentioned bifurcating parameters using phase portrait, Poincaré section, time and power spectra.

1. INTRODUCTION

This paper presents a study of the periodic and chaotic responses due to combination parametric resonance of a base excited cantilever beam carrying a lumped mass at an arbitrary position (Figure 1) which is an extension of the authors' work [1] where only the fixed point responses of the system were studied. The governing temporal equation of motion of the system is given by [1]

$$\ddot{u}_n + 2\varepsilon\zeta_n\dot{u}_n + \omega_n^2 u_n - \varepsilon\sum_{m=1}^{\infty} f_{nm}u_m\cos\phi\tau + \varepsilon\sum_{k=1}^{\infty}\sum_{l=1}^{\infty}\sum_{m=1}^{\infty}\{\alpha_{klm}^n u_k u_l u_m + \beta_{klm}^n u_k\dot{u}_l\dot{u}_m + \gamma_{klm}^n u_k u_l\ddot{u}_m\} = 0, \quad n = 1, 2, 3, \ldots \quad (1)$$

where $(\dot{\ })= \mathrm{d}(\ )/\mathrm{d}\tau$. The parameters ζ_n, ω_n represent the damping and natural frequency of the nth mode; f_{nm} is the forcing parameter in the nth mode due to the interaction of the mth mode; ϕ is the non-dimensional frequency of base

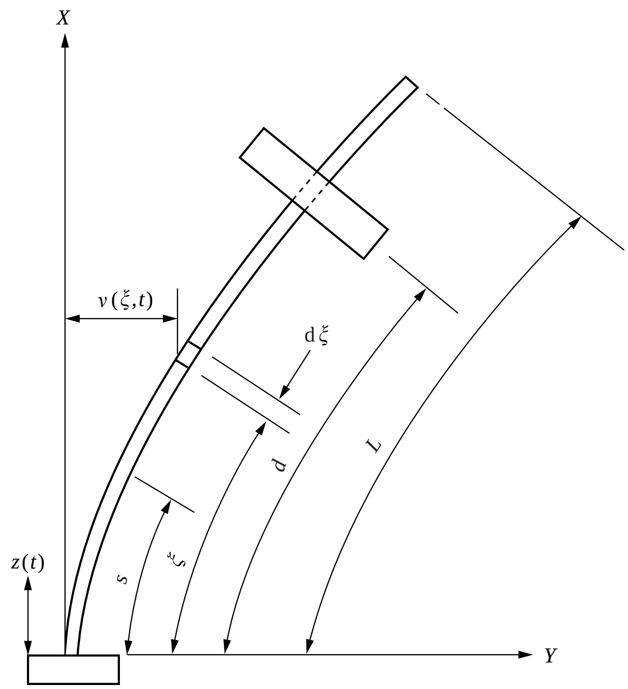

Figure 1. Vertically base-excited cantilever beam carrying a lumped mass.

excitation; α^n_{klm} is the coefficient of the geometric and β^n_{klm}, γ^n_{klm} are the coefficients of the inertial non-linear terms. The parameter ε is used to indicate the smallness of damping, forcing and non-linear terms.

There are a few studies available on the investigation of periodic and chaotic responses of parametrically excited systems with simultaneous combination and internal resonances. Asmis and Tso [2] investigated two-degree-of-freedom systems with cubic non-linearities to a combination parametric resonance and found beating effect for internal resonance of type 1:1. Nayfeh and Zavodney [3] obtained periodic orbits arising out of Hopf bifurcation and the sequence of period doubling leading to chaos for a two-degree-of-freedom system having quadratic non-linearities under combination parametric resonance with two-to-one internal resonances. The same system is further investigated by Streit *et al.* [4] where they found the non-zero periodic motions to co-exist with a stable equilibrium state over a range of detuning near the resonant frequency and also observed quenching of the chaotic motion near exact tuning to the parametric resonance. Nayfeh and Balachandran [5] reviewed the systems with modal interaction. Johnson and Bajaj [6] studied the amplitude modulated and chaotic dynamics in the resonant motion of strings, where they observed two limit cycle branches for the averaged equations, one arising due to the Hopf bifurcation and the other due to a global saddle-node bifurcation. With variation in detuning, the isolated branch exhibits period-doubling bifurcations, chaotic attractors and merging attractors, giving rise to Rössler as well as Lorentz-type solutions. Change in detuning also results in torus-doubling, merging of tori and then destruction of torus leading to chaotic amplitude modulations. Zavodney and Nayfeh [7] experimentally and theoretically dealt with principal parametric resonance of a base-excited cantilever beam carrying a lumped mass without internal resonance. Kar and Dwivedy [8] studied the same system [7] with an internal resonance of 3:1 and observed many chaotic phenomena. Banerjee *et al.* [9] obtained the periodic, chaotic responses of a two-degree-of-freedom system with quadratic non-linearity. Nayfeh and Balachandran [10] illustrated a number of examples related to the fixed-point, periodic, quasi-periodic and chaotic responses of different systems.

In most of these papers, either the method of multiple scales or the method of averaging is used to reduce the second order temporal equation to a set of first order differential equations which is then integrated to obtain periodic, quasi-periodic or chaotic responses. In this paper, the method of *normal forms* [11] is used to reduce the governing temporal equation (1) to a set of first order differential equations which is then directly integrated to get the periodic, quasi-periodic or chaotic response of the system. The purpose of using the method of normal form is to get the required results with simple mathematical substitution without going for the usual complicated mathematical formulation as in the case of the method of multiple scales [1, 3, 12–15] or the averaging method [4, 6, 9]. Poincaré section, time and power spectra are used to study these responses.

2. ANALYSIS

As a first step in determining uniform expansions of the solutions of equation (1) by the method of normal forms, we recast them into n first order complex valued equations. To accomplish this, the solution of this n-dimensional system with $\varepsilon = 0$ can be expressed as

$$u_n = A_n\,\mathrm{e}^{\mathrm{i}\omega_n\tau} + \bar{A}_n\,\mathrm{e}^{\mathrm{i}\omega_n\tau}, \tag{2}$$

where A_n are complex and $\bar{A}_n$ is the complex conjugate (cc) of A_n. Hence,

$$\dot{u}_n = \mathrm{i}\omega_n(A_n\,\mathrm{e}^{\mathrm{i}\omega_n\tau} - \bar{A}_n\,\mathrm{e}^{-\mathrm{i}\omega_n\tau}). \tag{3}$$

When $\varepsilon \neq 0$, u_n and $\dot{u}_n$ can still be represented by equations (2) and (3) but with time varying rather than constant A_n. Then identifying $A_n\,\mathrm{e}^{\,\mathrm{i}\omega_n\tau}$ by ξ_m, equations (2) and (3) can be rewritten as

$$u_m = \xi_m + \bar{\xi}_m, \quad \dot{u}_m = \mathrm{i}\omega_m(\xi_m - \bar{\xi}_m), \tag{4a, 4b}$$

where $\mathrm{i} = \sqrt{-1}$, ξ_m is a complex variable and $\bar{\xi}_m$ is its cc. Letting $z = \exp(\mathrm{i}\phi\tau)$ and substituting equations (4) into equation (1), one has

$$\dot{\xi}_n = \mathrm{i}\omega_n \xi_n - \varepsilon\zeta_n(\xi_n - \bar{\xi}_n) - \frac{\mathrm{i}\varepsilon}{4\omega_n}\sum_{m=1}^{\infty} f_{nm}(\xi_m + \bar{\xi}_m)(z + \bar{z})$$
$$+ \frac{\mathrm{i}\varepsilon}{2\omega_n}\sum_{klm}[\alpha^n_{klm}(\xi_k + \bar{\xi}_k)(\xi_l + \bar{\xi}_l)(\xi_m + \bar{\xi}_m)$$
$$- \omega_l\omega_m\beta^n_{klm}(\xi_k + \bar{\xi}_k)(\xi_l - \bar{\xi}_l)(\xi_m - \bar{\xi}_m)$$
$$+ \gamma^n_{klm}(\xi_k + \bar{\xi}_k)(\xi_l + \bar{\xi}_l)\{\omega_m^2(\bar{\xi}_m - \bar{\xi}_m) + 2\mathrm{i}\omega_m\dot{\xi}_m\}]. \tag{5}$$

To simplify the above equation, introduce the near-identity transformation

$$\xi_n = \eta_n + \varepsilon h_n(\eta_m, \bar{\eta}_m, z, \bar{z}). \tag{6}$$

Substitution of equation (6) into equation (5) yields

$$\dot{\eta}_n = \mathrm{i}\omega_n(\eta_n + \varepsilon h_n) - \varepsilon\zeta_n(\eta_n - \bar{\eta}_n) + \frac{\mathrm{i}\varepsilon}{4\omega_n}\sum_{m=1}^{\infty} f_{nm}(z + \bar{z})(\eta_m + \bar{\eta}_m)$$
$$- \varepsilon\sum_{m=1}^{\infty}\left(\frac{\partial h_n}{\partial \eta_m}\dot{\eta}_m + \frac{\partial h_n}{\partial \bar{\eta}_m}\dot{\bar{\eta}}_m\right) - \varepsilon\left(\frac{\partial h_n}{\partial z}\dot{z} + \frac{\partial h_n}{\partial \bar{z}}\dot{\bar{z}}\right)$$
$$+ \frac{\mathrm{i}\varepsilon}{2\omega_n}\sum_{klm}[\alpha^n_{klm}(\eta_k + \bar{\eta}_k)(\eta_l + \bar{\eta}_l)(\eta_m + \bar{\eta}_m)$$
$$- \omega_l\omega_m\beta^n_{klm}(\eta_k + \bar{\eta}_k)(\eta_l - \bar{\eta}_l)(\eta_m - \bar{\eta}_m)$$
$$+ \gamma^n_{klm}(\eta_k + \bar{\eta}_k)(\eta_l + \bar{\eta}_l)\{\omega_m^2(\eta_m - \bar{\eta}_m) + 2\mathrm{i}\omega_m\dot{\eta}_m\}] + O(\varepsilon^2). \tag{7}$$

The form of the $O(\varepsilon)$ terms suggests the following form of h_m

$$h_m = \Delta_{m1}\eta_m + \Delta_{m2}\bar{\eta}_m + \sum_{k=1}^{\infty}[\Gamma^1_{mk} z\eta_k + \Gamma^2_{mk} z\bar{\eta}_k + \Gamma^3_{mk}\bar{z}\eta_k + \Gamma^4_{mk}\bar{z}\bar{\eta}_k]. \tag{8}$$

It follows from equation (7) that

$$\dot{\eta}_n = \mathrm{i}\omega_n\eta_n + O(\varepsilon). \tag{9}$$

Substituting equations (8) and (9) into equation (7), one has

$$
\begin{aligned}
\dot{\eta}_n = {} & \mathrm{i}\omega_n\eta_n - \varepsilon\zeta_n\eta_n + \varepsilon(\zeta_n + 2\mathrm{i}\omega_n\Delta_{n2})\bar{\eta}_n \\
& + \mathrm{i}\varepsilon\sum_{k=1}^{\infty}\left[\left\{(\omega_n - \omega_k - \phi)\Gamma^1_{nk} - \frac{1}{4\omega_n}f_{nk}\right\}z\eta_k\right. \\
& + \left\{(\omega_n + \omega_k - \phi)\Gamma^2_{nk} - \frac{1}{4\omega_n}f_{nk}\right\}z\bar{\eta}_k \\
& + \left\{(\omega_n - \omega_k + \phi)\Gamma^3_{nk} - \frac{1}{4\omega_n}f_{nk}\right\}\bar{z}\eta_k \\
& \left. + \left\{(\omega_n + \omega_k + \phi)\Gamma^4_{nk} - \frac{1}{4\omega_n}f_{nk}\right\}\bar{z}\bar{\eta}_k\right] \\
& + \frac{\mathrm{i}\varepsilon}{2\omega_n}\sum_{klm}\left[\left\{\alpha^n_{klm} - \omega_m^2\gamma^n_{klm}\right\}(\eta_k + \bar{\eta}_k)(\eta_l + \bar{\eta}_l)(\eta_m + \bar{\eta}_m)\right. \\
& \left. - \omega_l\omega_m\beta^n_{klm}(\eta_k + \bar{\eta}_k)(\eta_l - \bar{\eta}_l)(\eta_m - \bar{\eta}_m)\right]. \qquad (10)
\end{aligned}
$$

Inserting equation (6) into equation (4), one gets

$$u_m = \eta_m + \bar{\eta}_m + O(\varepsilon). \qquad (11)$$

Note that equation (10) does not contain terms Δ_{n1}; hence, they are arbitrary. Choosing Γ^i_{nk}, $i = 1, 2, 3, 4$ to eliminate the terms involving $z\eta_n$, $z\bar{\eta}_n$, $\bar{z}\eta_n$ and $\bar{z}\bar{\eta}_n$, it is found that some of Γ^i_{nk} have small-divisor terms for combination resonance and the coefficients of non-linear terms have small-divisor terms for internal resonance, which are discussed in the next section.

2.1. COMBINATION RESONANCE ($\phi \approx \omega_1 + \omega_2$)

Since $\omega_2 \approx 3\omega_1$, to express the nearness of ϕ to $\omega_1 + \omega_2$ the detuning parameters σ_1 and σ_2 are introduced as

$$\omega_2 = 3\omega_1 + \varepsilon\sigma_2, \quad \phi = 4\omega_1 + \varepsilon\sigma_1 = \omega_1 + \omega_2 + \varepsilon(\sigma_1 - \sigma_2). \qquad (12)$$

Substituting equations (12) into equation (10) and eliminating the secular terms, one has for $n = 1$,

$$\dot{\eta}_1 = \mathrm{i}\omega_1\eta_1 - \varepsilon\zeta_1\eta_1 - \frac{\mathrm{i}\varepsilon}{4\omega_1}f_{12}z\bar{\eta}_2 + \frac{\mathrm{i}\varepsilon}{2\omega_1}\left[\sum_{j=1}^{\infty}\alpha_{e1j}\eta_1\bar{\eta}_j\eta_j + Q_1\eta_2\bar{\eta}_1^2\right] \qquad (13)$$

for $n = 2$,

$$\dot{\eta}_2 = \mathrm{i}\omega_2\eta_2 - \varepsilon\zeta_2\eta_2 - \frac{\mathrm{i}\varepsilon}{4\omega_2}f_{21}z\bar{\eta}_1 + \frac{\mathrm{i}\varepsilon}{2\omega_2}\left[\sum_{j=1}^{\infty}\alpha_{e2j}\eta_2\bar{\eta}_j\eta_j + Q_2\eta_1^3\right] \qquad (14)$$

and for $n > 2$.

$$\dot{\eta}_n = \mathrm{i}\omega_n\eta_n - \varepsilon\zeta_n\eta_n + \frac{\mathrm{i}\varepsilon}{2\omega_n}\sum_{j=1}^{\infty}\alpha_{enj}\eta_n\bar{\eta}_j\eta_j, \tag{15}$$

where the expressions for Q_i and α_{eij}, $i = 1, 2, \dots, j = 1, 2, \dots$ are given in Appendix A. As the higher modes ($n > 2$) are neither directly excited nor indirectly excited by internal resonance, they die out due to the presence of damping. So, for this case, our n-dimensional system reduces to a two-dimensional one as modal interaction is limited to two modes only. Comparing equations (2) and (11) and introducing

$$A_n = \frac{1}{2}a_n(\tau)\exp\{\mathrm{i}\beta_n(\tau)\}, \tag{16}$$

one has

$$\eta_n = \frac{1}{2}a_n\exp\{\mathrm{i}(\omega_n\tau + \beta_n)\}, \tag{17}$$

where, a_n and β_n are real. Substituting equation (17) into equations (13–15) and separating the real and imaginary parts, one has the following set of autonomous equations.

$$2\omega_1(\zeta_1 a_1 + \dot{a}_1) - \frac{1}{2}f_{12}a_2\sin\gamma_1 + \frac{1}{4}Q_1 a_2 a_1^2\sin\gamma_2 = 0 \tag{18}$$

$$-\omega_1 a_1(\sigma_1 - \dot{\gamma}_1 - \dot{\gamma}_2) - f_{12}a_2\cos\gamma_1 + \frac{1}{2}\sum_{j=1}^{2}\alpha_{e1j}a_j^2 a_1 + \frac{1}{2}Q_1 a_2 a_1^2\cos\gamma_2 = 0, \tag{19}$$

$$2\omega_2(\zeta_2 a_2 + \dot{a}_2) - \frac{1}{2}f_{21}a_1\sin\gamma_1 - \frac{1}{4}Q_2 a_1^3\sin\gamma_2 = 0, \tag{20}$$

$$-\omega_2 a_2(3\sigma_1 - 4\sigma_2 - \dot{\gamma}_2 - 3\dot{\gamma}_1) - f_{21}a_1\cos\gamma_1 + \frac{1}{2}\sum_{j=1}^{2}\alpha_{e2j}a_j^2 a_2 + \frac{1}{2}Q_2 a_1^3\cos\gamma_2 = 0, \tag{21}$$

where

$$\gamma_1 = -\beta_1 + \frac{1}{4}\sigma_1\tau, \quad \gamma_2 = -\beta_2 - \left(\sigma_2\tau - \frac{3}{4}\sigma_1\tau\right). \tag{22, 23}$$

The same set of reduced equations (18–21) have been obtained using the method of multiple scales [1].

The first order solutions of the system can be given by

$$u_1 = a_1\cos\{\bar{\omega}_1\tau - \gamma_1\}, \quad u_2 = a_2\cos\{\bar{\omega}_2\tau - \gamma_2\}, \tag{24a, 24b}$$

where

$$\bar{\omega}_1 = \omega_1 + \varepsilon\sigma_1/4 \quad \bar{\omega}_2 = 3\bar{\omega}_1. \tag{25a 25b}$$

While finding the stability and bifurcation of the steady state response, as the reduced equations (18–21) contain terms $a_i\dot{\gamma}_j(i\ j = 1\ 2)$, their perturbed equations will not contain the perturbations $\Delta\dot{\gamma}_1$ or $\Delta\dot{\gamma}_2$ for trivial solutions. Hence, stability of trivial points cannot be obtained by perturbing the above reduced equations. Hence, to overcome this difficulty, the transformation

$$p_i = a_i \cos\gamma_i \quad q_i = a_i \sin\gamma_i \tag{26a 26b}$$

is introduced and trigonometric manipulations are carried out to arrive at the following normalized reduced equations.

$$2\omega_1\left(\dot{p}_1 + \zeta_1 p_1 + \frac{1}{4}\sigma_1 q_1\right) - \frac{1}{2}\,f_{12}q_2 - \frac{1}{4}\sum_{j=1}^{2}\alpha_{e1j}q_1(p_j^2 + q_j^2) + \frac{1}{4}Q_1\{q_2(q_1^2 - p_1^2) + 2p_1p_2q_1\} = 0 \tag{27a}$$

$$2\omega_1\left(\dot{q}_1 + \zeta_1 q_1 - \frac{1}{4}\sigma_1 p_1\right) - \frac{1}{2}\,f_{12}p_2 + \frac{1}{4}\sum_{j=1}^{2}\alpha_{e1j}p_1(p_j^2 + q_j^2) + \frac{1}{4}Q_1\{p_2(p_1^2 - q_1^2) + 2p_1q_1q_2\} = 0 \tag{27b}$$

$$2\omega_2\left\{\dot{p}_2 + \zeta_2 p_2 - \left(\sigma_2 - \frac{3}{4}\sigma_1\right)q_2\right\} - \frac{1}{2}\,f_{21}q_1 - \frac{1}{4}Q_2\{q_1(3p_1^2 - q_1^2)\} - \frac{1}{4}\sum_{j=1}^{2}\alpha_{e2j}q_2(p_j^2 + q_j^2) = 0 \tag{27c}$$

$$2\omega_2\left\{\dot{q}_2 + \zeta_2 q_2 + \left(\sigma_2 - \frac{3}{4}\sigma_1\right)p_2\right\} - \frac{1}{2}\,f_{21}p_1 + \frac{1}{4}Q_2\{p_1(p_1^2 - 3q_1^2)\} + \frac{1}{4}\sum_{j=1}^{2}\alpha_{e2j}p_2(p_j^2 + q_j^2) = 0. \tag{27d}$$

Using equations (26), equation (24) can be rewritten as

$$u_1 = p_1\cos\bar{\omega}_1\tau + q_1\sin\bar{\omega}_1\tau \quad u_2 = p_1\cos 3\bar{\omega}_1\tau + q_1\sin 3\bar{\omega}_1\tau \tag{28a 28b}$$

where

$$\bar{\omega}_1 = \omega_1 + \varepsilon\sigma_1/4.$$

2.2. STABILITY OF PERIODIC RESPONSE

Stability of the periodic solutions of the modulation equations (27) is determined using Floquet theory. Thus, to determine the stability of a T periodic limit cycle $\mathbf{P}(\tau) = \mathbf{P}(\tau + T)$, where $P = [p_1, q_1, p_2, q_2]^T$, one superimposes on it a small perturbation $\theta(\tau)$. Expanding the resulting equation in Taylor series for small $\theta(\tau)$ and linearizing the flow about the periodic orbit, one obtains the linear variational equation

$$\dot{\theta} = J_c(\tau)\theta, \tag{29}$$

where J_c is the Jacobian matrix of equation (27).

Let $\boldsymbol{\Theta}(\tau)$ be the fundamental-matrix solution satisfying

$$\dot{\boldsymbol{\Theta}} = J_c(\tau)\boldsymbol{\Theta}, \quad \boldsymbol{\Theta}(0) = I. \tag{30}$$

where I is the unit matrix.

Then, the Floquet multipliers are the eigenvalues of the monodromy matrix $\boldsymbol{\Theta}(T)$. Because equations (27) are autonomous, one of the multipliers is always $+1$. If all the other multipliers lie inside the unit circle, then the orbit is asymptotically stable. If one of the multipliers leaves the unit circle, then the orbit is unstable. When a multipler leaves the unit circle through $+1$, the resulting bifurcation is either cyclic-fold or pitchfork, when it leaves through -1, period-doubling bifurcation occurs. A Hopf or Neimark bifurcation occurs when two complex conjugate multipliers leave the unit circle.

3. NUMERICAL RESULTS AND DISCUSSION

In part I of this paper [1], the fixed point response of the reduced equations are studied extensively for different system parameters and it is shown that the fixed point response loses its stability either by saddle-node (s-n) or by Hopf bifurcation point (HBP) under combination parametric and internal resonances of type 3:1. Though these response curves predict the regions in which the fixed-point responses are unstable, it is not determined whether the system is stable or unstable in that region, because in these regions the system may have stable periodic or quasi-periodic response, or the response may be chaotic depending on the control parameters (namely, amplitude of base excitation Γ, external and internal detuning parameters σ_1, σ_2 and damping parameter ν). Also, in between the stable fixed-points for a given set of control parameters, the system may have periodic, quasi-periodic or chaotic attractors. Hence, the overall stability of the system can be predicted only when all other possible responses are determined along with its fixed-point response. Besides, the system response may change abruptly with the variation of the system parameters. Hence, in this section a parametric study of the periodic, quasi-periodic and chaotic responses is carried out.

As the periodic, quasi-periodic and chaotic responses have their local/global origin at the fixed point responses, to start with, the critical points are determined from frequency and forced response curves by numerically solving the reduced equations (18–21), and their stability and bifurcation are obtained from the eigenvalues of the Jacobian matrix J_c. It may be noted from equations (24) and (28) that the fixed point response of the reduced equations corresponds to the periodic response of the original system.

Figure 2 shows the bifurcation set in the $\Gamma \sim \phi$ plane for damping parameter $\nu = 2$. To better visualize these bifurcation points, response curves for some values of Γ are plotted in Figure 3. As the same bifurcations are observed in both modes, only the first mode non-trivial response curves are plotted in Figure 3. The trivial response can be determined from Figure 2, which is unstable between the two Hopf bifurcation points. While THBP(L) and THBP(R) represent respectively the set of sub- and super-critical HBP to the left and right of the unstable branch of the trivial state, NTHBP(L) and NTHBP(R) represent the set of super- and sub-critical Hopf bifurcation points in the non-trivial branch. The THBP(L) and THBP(R) coalesce at $\phi = \omega_1 + \omega_2$ with $\Gamma = 4{\cdot}74$. Though the trivial state is completely stable below $\Gamma = 4{\cdot}74$, the non-trivial responses exist much below this value. But, these non-trivial branches are unstable below $\Gamma = 4$, the critical point at which the first nucleation of a stable point is observed in the response curve (Figure 3, curve a) at $\phi = \omega_1 + \omega_2$ with the generation of NTHBP(R). With an increase in Γ, this closed curve becomes increased in size and another isolated curve to the left of it appears with the stable and unstable branches meeting at the s-n bifurcation point (Figure 2, curve 4). Also, in the lower side of the closed curve one stable branch is observed having s-n bifurcations at the ends (starting points of 6 and 7, Figure 1). Further increase in Γ gives birth to the NTHBP(L) and another s-n point in the original

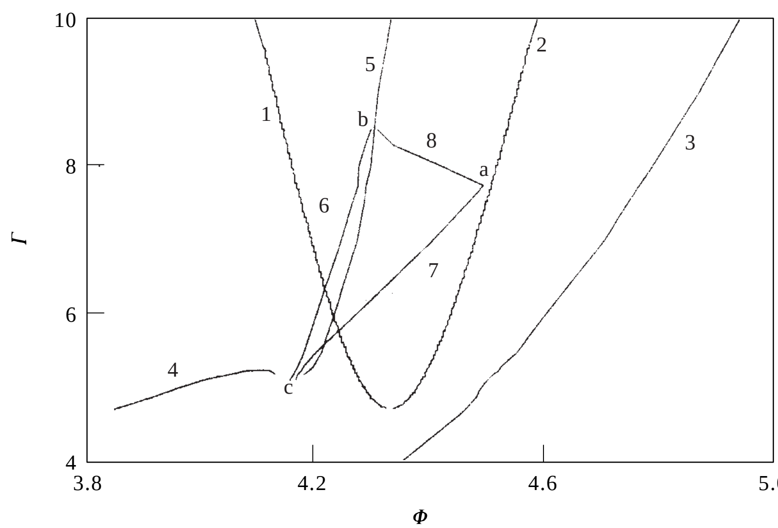

Figure 2. Bifurcation set with $\nu = 2$. Lines 1—THBP(L), 2—THBP(R), 3—NTHBP(R), 4—s-n, 5—NTHBP(L); 6, 7 and 8 s-n.

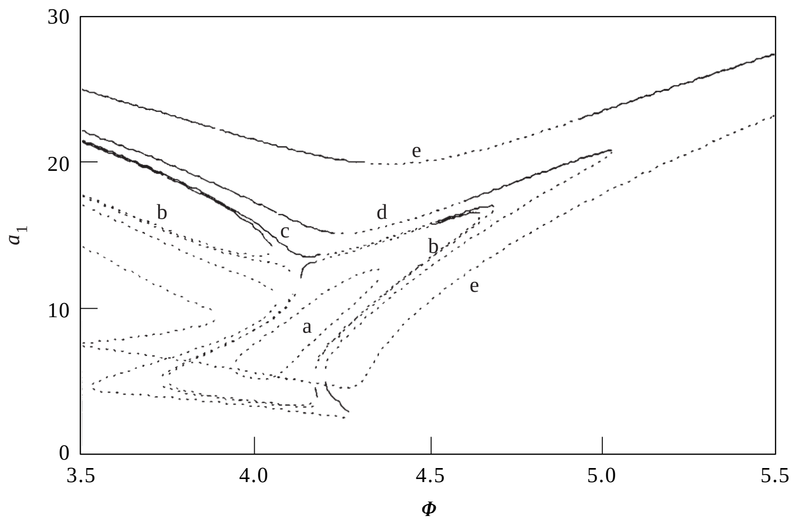

Figure 3. Frequency response curves with $\nu = 2$. (a) $\Gamma = 4$, (b) $\Gamma = 5{\cdot}2$, (c) $\Gamma = 5{\cdot}3$, (d) $\Gamma = 6$, (e) $\Gamma = 10$.

closed curve (Figure 3, curve b) which, with a higher value of Γ, becomes the meeting point of these two isolated curves (Figure 3, curve c). The stable branch in the lower side of the response curve increases till it reaches the domain of THBP(R), after which (point "a" Figure 1) it decreases sharply and the two s-n points coalesce at point "b" (Figure 2), where they meet the NTHBP(L). As this stable branch exists to the right of NTHBP(L), the system has a tendency to jump to it from the NTHBP(L). With an increase in Γ, the single response curve (Figure 3, curve d) is divided into the upper and lower branches (Figure 3, curve e). The lower branch is purely unstable with many turning points (not s-n) which play a significant role in the creation of the periodic, quasi-periodic and chaotic orbits. As topologically equivalent bifurcation sets are observed for different values of ν, they are not plotted here.

Considering the response curve at $\Gamma = 6$ and $\nu = 2$, the system has a sub-critical HBP ($\phi = 4{\cdot}22$) to the left of the unstable trivial state, and hence the response will jump to the stable non-trivial branch which loses its stability at the s-n ($\phi = 4{\cdot}27$) bifurcation point and an *isolated stable periodic orbit* having its global origin at this s-n bifurcation point, similar to those found by Johnson and Bajaj [6], is observed. With an increase in the frequency of external excitation ϕ, the periodic orbit becomes reduced in size (Figure 4) as it approaches the super-critical THBP(R) (Figure 2). From Figure 4, it can be observed that the amplitudes of the second mode periodic orbits are approximately twice those of the first mode. As the amplitude of external excitation Γ increases, for the given ϕ and ν, these periodic orbits initially increase in size and suddenly disappear giving rise to *blue-sky catastrophe* as Γ enters the s-n triangle (Figure 2, triangle abc), which again appear when Γ comes out of the s-n triangle. These variations in periodic orbits are shown in Figure 5 for $\phi = 4{\cdot}3$ and $\nu = 2$. Though these orbits are periodic, they contain many harmonics. With further increase in

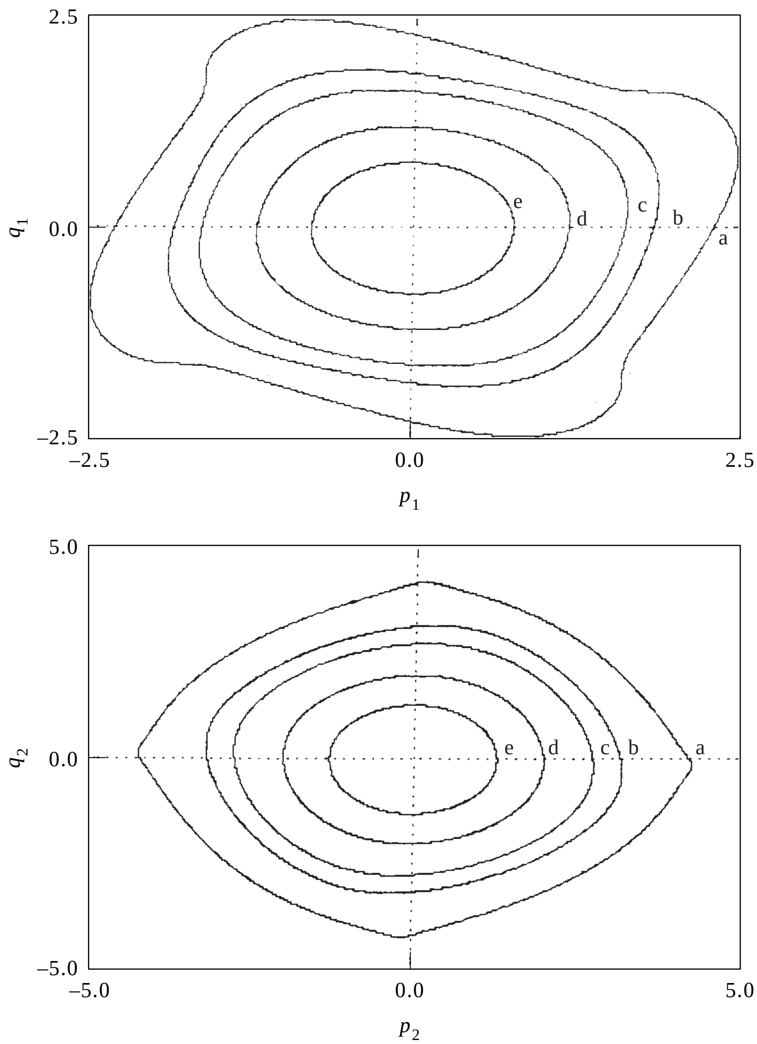

Figure 4. Periodic orbits near the super-critical trivial Hopf bifurcation point (THBP(R)). $\Gamma = 6$, $\nu = 2$; a: $\phi = 4{\cdot}3$, b: $\phi = 4{\cdot}35$, c: $\phi = 4{\cdot}37$, d: $\phi = 4{\cdot}4$, e: $\phi = 4{\cdot}42$.

$\Gamma(\Gamma \geqslant 10)$, these periodic orbits finally escape to another periodic orbit having its global bifurcation point at the NTHBP(L) (Figure 6).

Figure 6 shows the four symmetrically placed periodic orbits along with the limit cycle at the trivial fixed point for $\phi = 4{\cdot}3$, $\Gamma = 10$, $\nu = 2$. While equations (27) indicate $(p_1, q_1, p_2, q_2) \Leftrightarrow (-p_1, -q_1, -p_2, -q_2)$ is the only possible transformation, numerical calculations give the following transformation for the periodic attractors:

$$\begin{aligned}(p_1, q_1, p_2, q_2) &\Leftrightarrow (-q_1, p_1, q_2, -p_2) \Leftrightarrow (q_1, -p_1, -q_2, p_2)\\ &\Leftrightarrow (-p_1, -q_1, -p_2, -q_2).\end{aligned}$$

Though the response curve (Figure 3, for $\Gamma = 10$) shows the NTHBP(L) at $\phi = 4{\cdot}32$, due to strong interaction of the fold at $\phi = 4{\cdot}28$, isolated periodic

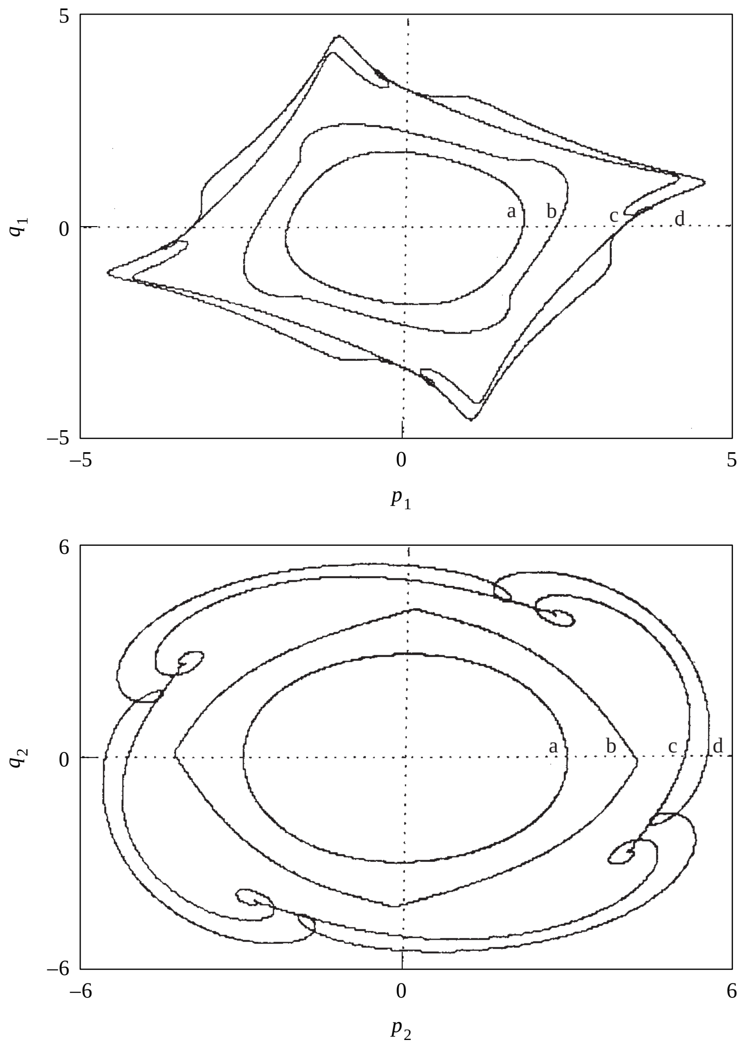

Figure 5. Variation of periodic orbits having their global origin at THBP(R) with Γ. ϕ = 4·3, ν = 2; a: Γ = 5, b: Γ = 6, c: Γ = 9, Γ = 10.

orbits are observed (Figure 7) slightly before NTHBP(L). The cross (i.e., eight shape) in the second mode of the state space is due to the presence of harmonics. The time response clearly indicates that the system exhibits *mixed-mode oscillation* which can be represented by P_1^1, i.e., a large-amplitude oscillation is followed by a small-amplitude oscillation [10]. The power spectra also indicate the presence of harmonics in the response.

With an increase in ϕ, *period doubling* takes place (Figure 8) as one of the Floquet multiplier leaves the unit circle through -1. This periodic oscillation is again a *mixed-mode oscillation* of type P_2^2. Unlike the case of principal parametric resonance [8], here the period doubling does not lead to chaos as the 2T-period reverts back to single period. The 2T-periodic orbits and their time spectra at ϕ = 4·45, Γ = 10 and ν = 2, and the periodic orbit at ϕ = 4·56 with

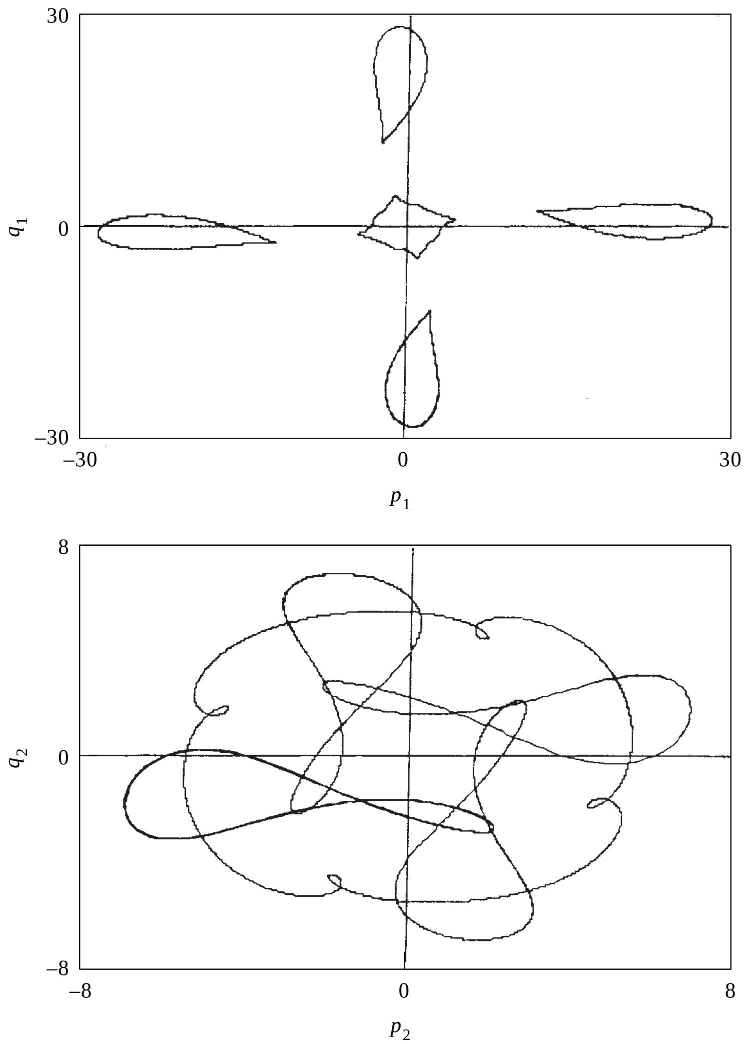

Figure 6. Simultaneous existence of periodic orbits near the trivial and non-trivial super critical Hopf bifurcation points. $\Gamma = 10$, $\phi = 4{\cdot}3$, $\nu = 2$.

the same Γ and ν are shown in Figure 9. These periodic orbits, with an increase in ϕ, continue till they reach the domain of the sub-critical NTHBP(R). Further increase in ϕ results in the *blue-sky catastrophe* with sudden disappearance of the periodic orbits, and the response jumps down to the stable trivial fixed point.

For r ≈ 5, $\nu \approx 0{\cdot}03$ and at $\phi = 4$, the *beating effect* is observed, which dies down with the passage of time (Figure 10).

It has already been shown in Figure 6 that four symmetrically placed periodic attractors are found near the THBP(R) for higher values of ν (e.g., $\nu = 2$). It is observed that, with a decrease in ν, the size of these periodic attractors decreases and they move towards the origin (i.e., the trivial fixed point). One such periodic attractor is shown in Figure 11(a) (marked by 1) and its time response is shown in (b). For $\Gamma = 10$ and $\phi = 4{\cdot}3$, these periodic attractors exist up to $\nu = 1{\cdot}6$. These mixed-mode periodic responses, with further decrease in damping, change

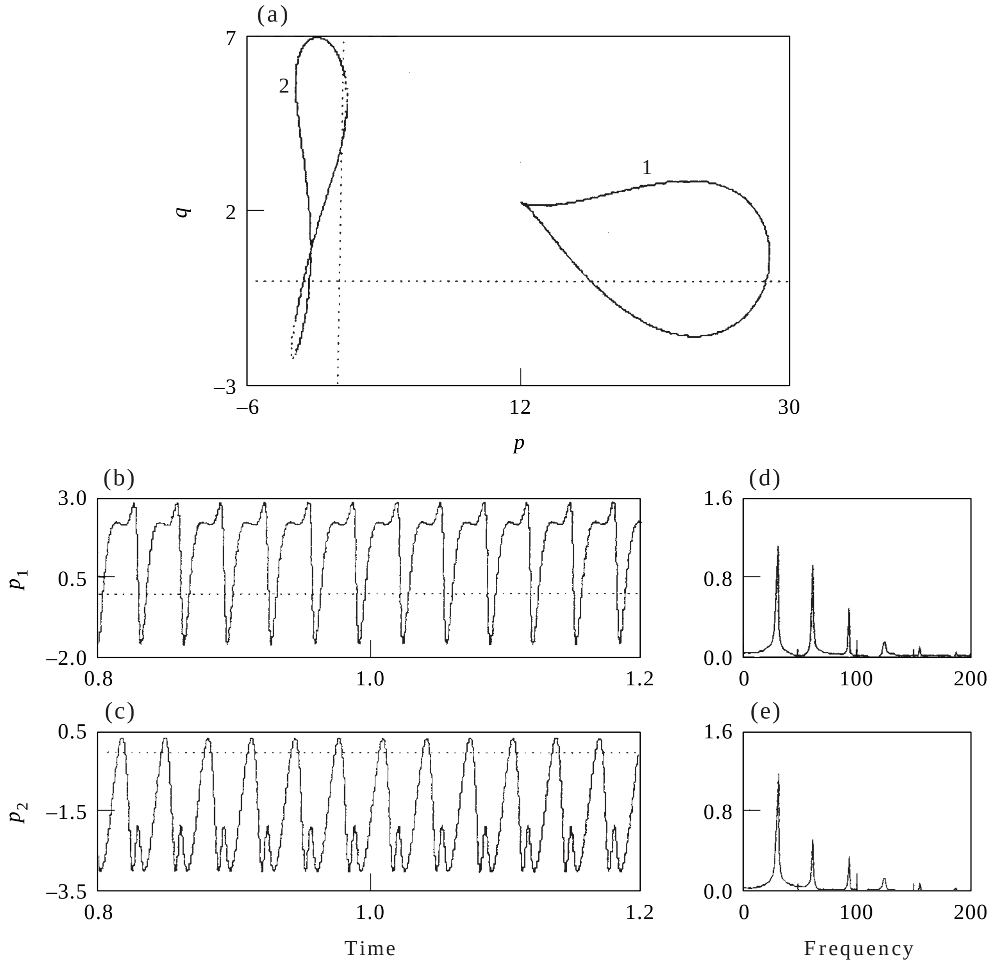

Figure 7. Mixed-mode periodic orbit near the NTHBP(L) for $\Gamma = 10$, $\phi = 4{\cdot}28$, $\nu = 2$. (a) Phase portrait, (b, c) time spectra and (d, e) corresponding power spectra.

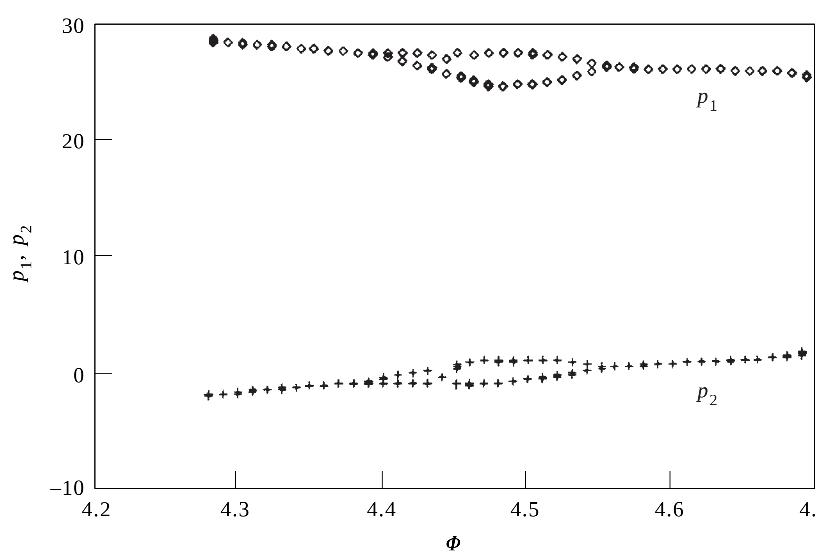

Figure 8. Poincaré section showing variation of periodic orbits between super- and sub-critical non-trivial Hopf bifurcation points.

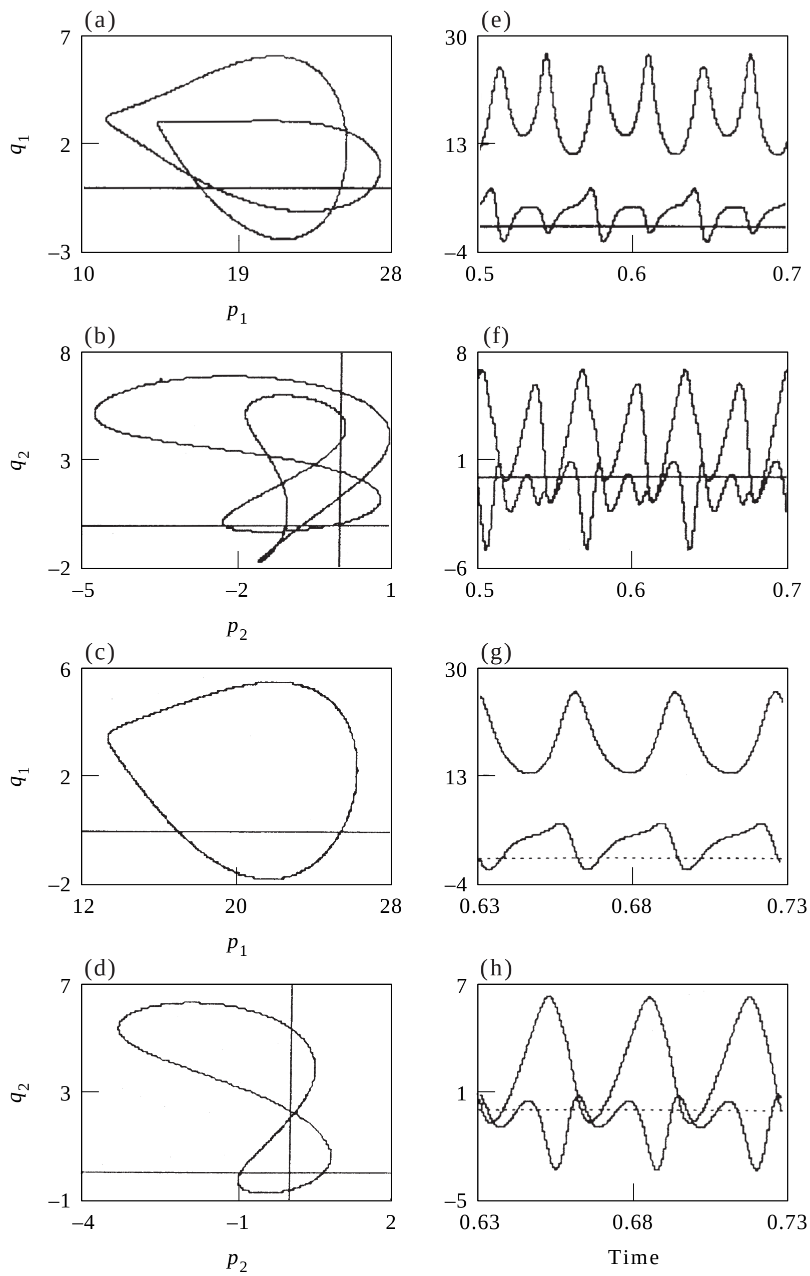

Figure 9. Phase portrait and corresponding time spectra with $\Gamma = 10$, $\nu = 2$. (a, b, e, f) $\phi = 4{\cdot}45$, (c, d, g, h) $\phi = 4{\cdot}56$.

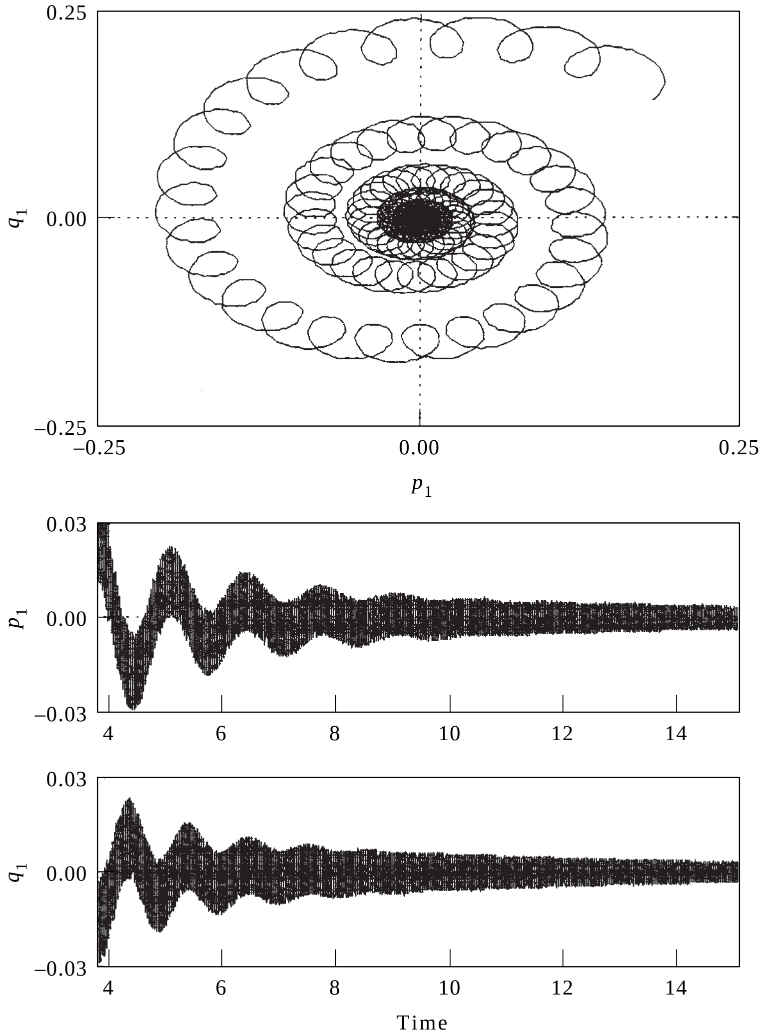

Figure 10. Phase portrait showing beating effect for $\phi = 4$, $\Gamma = 4{\cdot}5$, $\nu = 0{\cdot}03$.

to chaotic ones which are a random mixture of the nearby periodic states. Such a sequence is known as an *alternate periodic-chaotic sequence* which continues till ν reaches 0·7. One such chaotic attractor at $\nu = 0{\cdot}75$ is marked by 2 in Figure 11(a) and its time response is shown in Figure 11(c). As these chaotic attractors come closer to each other with further decrease in ν, one of the chaotic orbits visits intermittently the other chaotic orbits, and returns back to the phantom (or ghost) orbit (Figure 11) and the corresponding time response (Figure 11(d)) is interrupted by sudden chaotic outbursts. This is a new type of intermittency route to chaos which is preceded by alternate periodic-chaotic sequence of the mixed-mode periodic response. All these four chaotic orbits have a tendency to merge and form a bigger chaotic attractor giving rise to *attractor merging crisis* (Figure 12).

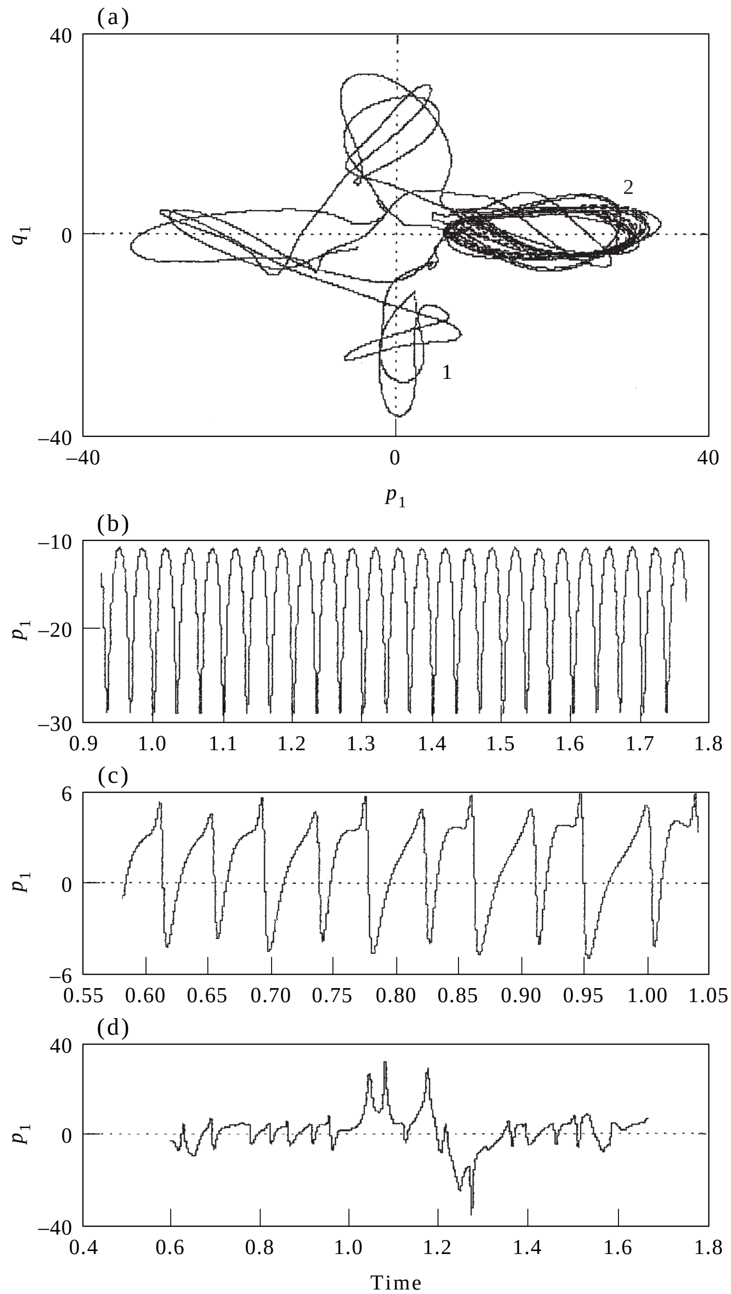

Figure 11. Phase portrait and time spectra showing alternate periodic chaotic sequence and intermittency route to chaos. $\Gamma = 10$, $\phi = 4{\cdot}3$; 1: $\nu = 1{\cdot}75$, 2: $\nu = 0{\cdot}75$, 3: $\nu = 0{\cdot}6$.

Besides these periodic responses, the system also experiences quasi-periodic responses in the region where the system has stable fixed points. For the undamped system and with an external frequency far away from $\phi = \omega_1 + \omega_2$, two-torus orbits have been observed. One such torus for $\phi = 3{\cdot}5$, $\Gamma = 10$ is shown in Figure 13(a) and its Poincaré section is shown in Figure 13(d). Figure

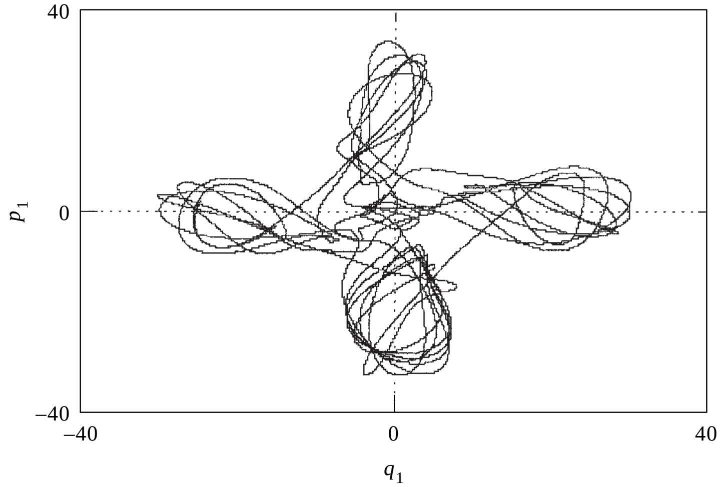

Figure 12. Attractor merging crisis at $\phi = 4{\cdot}3$, $\Gamma = 10$, $\nu = 0$.

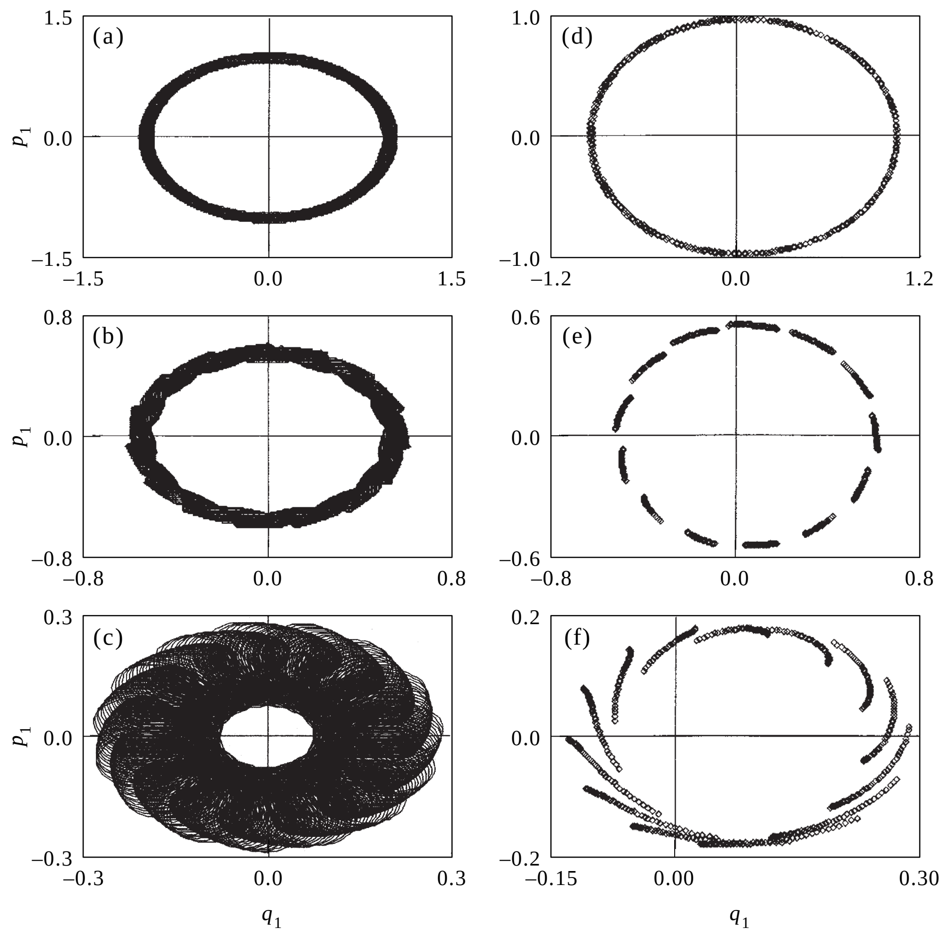

Figure 13. Different responses for $\phi = 3{\cdot}5$, $\Gamma = 10$. (a) Quasi-periodic orbit with initial condition (ic) (1·0, −0·34, 3·14, 5·23); (b) chaotic response due to broken torus with ic (0·6, −0·34, 3·14, 6·28), and (c) chaotic response with ic (0·23, −0·34, 3·14, 6·28); (d), (e) and (f) are the corresponding Poincaré sections.

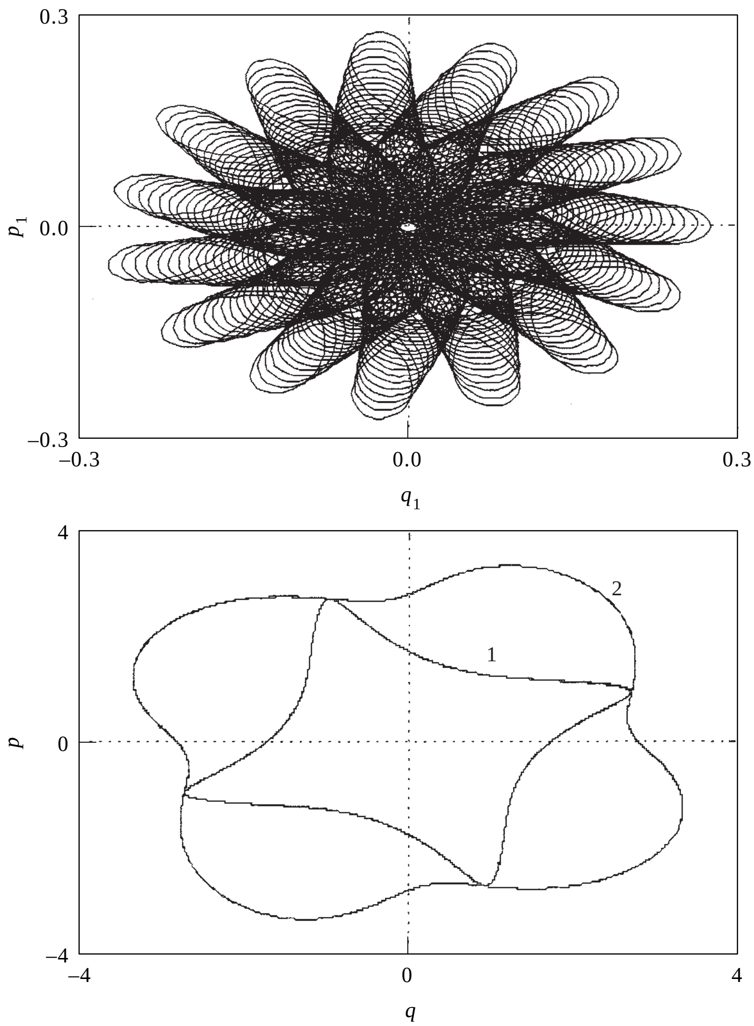

Figure 14. Effect of damping with $\Gamma = 10$, $\phi = 4{\cdot}3$. (a) Torus breakdown route to chaos: $\nu = 0{\cdot}01$; (b) periodic response: $\nu = 1$.

13(b) shows the chaotic response arising out of a broken torus (Figure 13(e)). With a slight change in the initial conditions another interesting chaotic attractor (Figure 13(c)) is obtained whose Poincaré section is shown in Figure 13(f). This clearly indicates the *butterfly effect* of the chaotic attractor.

With an increase in damping, breakdown of the tori takes place (Figure 14(a)) leading to chaotic responses. With further increase in damping this chaotic attractor comes into contact with the trivial fixed point response and becomes periodic. Figure 14(b) shows the periodic attractor which exists for $\nu = 1$.

With variations in μ and β, similar observations have been made for periodic, quasi-periodic and chaotic responses, the only change being in their global origins.

4. CONCLUSIONS

The method of normal form is used to determine the dynamic response of a slender beam with a lumped mass at an arbitrary position subjected to combination parametric and internal resonances of 3:1. The system has cubic geometric and inertial non-linearities. The bifurcation set for the fixed-point response indicating the Hopf bifurcation sets for the trivial and non-trivial states and the s-n triangle in between the unstable trivial states are clearly marked with reference to the response curves for a wide range of Γ. These bifurcation points play an important role in the nucleation of periodic, quasi-periodic and chaotic orbits. Variation of the periodic orbits with their global origin from the s-n and Hopf bifurcation points with Γ, ϕ and ν are studied. Mixed-mode oscillation, period-doubling, quasi-periodic orbits and different routes to chaos, namely, alternate periodic-chaotic transition, torus break-down and intermittency, are observed along with the attractor merging crisis and butterfly effect. These responses are analyzed using phase portraits, Poincaré sections, time and power spectra.

REFERENCES

1. S. K. Dwivedy and R. C. Kar 1999 *Journal of Sound and Vibration* **221**, 823–848. Dynamics of a slender beam with an attached mass under combination parametric and internal resonances. Part I: steady state response.
2. K. G. Asmis and W. K. Tso 1972 *ASME*, *Journal of Applied Mechanics* **39**, 832–834. Combination and internal resonance in a non-linear two-degree-of-freedom system.
3. A. H. Nayfeh and L. D. Zavodney 1986 *Journal of Sound and Vibration* **107**, 329–350. The response of two degree-of-freedom systems with quadratic non-linearities to a combination parametric resonance.
4. D. A. Streit, A. K. Bajaj and C. M. Krousgrill 1988 *Journal of Sound and Vibration* **124**, 297–314. Combination parametric resonance leading to periodic and chaotic response in two-degree-of-freedom systems with quadratic non-linearities.
5. A. H. Nayfeh and B. Balachandran 1989 *ASME*, *Applied Mechanics Review* **42**, S175–S201. Modal interactions in dynamical and structural systems.
6. J. M. Johnson and A. K. Bajaj 1989 *Journal of Sound and Vibration* **128**, 87–107. Amplitude modulated and chaotic dynamics in resonant motion of strings.
7. L. D. Zavodney and A. H. Nayfeh 1989 *International Journal of Non-linear Mechanics* **24**, 105–125. The non-linear response of a slender beam carrying a lumped mass to principal parametric excitation: theory and experiment.
8. R. C. Kar and S. K. Dwivedy 1999 *International Journal of Nonlinear Mechanics* **34**, 515–529. Nonlinear dynamics of a slender beam carrying a lumped mass with principal parametric and internal resonances.
9. B. Banerjee, A. K. Bajaj and P. Davies 1996 *International Journal of Non-linear Mechanics* **31**, 21–39. Resonant dynamics of an autoparametric system: a study using higher-order averaging.

10. A. H. NAYFEH and B. BALACHANDRAN 1995 *Applied Nonlinear Dynamics*. New York: Wiley-Interscience.
11. A. H. NAYFEH 1993 *Method of Normal Forms*. New York: Wiley-Interscience.
12. A. H. NAYFEH 1983 *Journal of Sound and Vibration* **88**, 547–557. The response of two-degree-of-freedom systems with quadratic non-linearities to a parametric excitation.
13. A. H. NAYFEH 1983 *Journal of Sound and Vibration* **90**, 237–244. The response of multi-degree-of-freedom systems with quadratic non-linearities to a harmonic parametric resonance.
14. A. H. NAYFEH and P. F. PAI 1989 *International Journal of Non-linear Mechanics* **24**, 139–158. Non-linear non-planar parametric responses of an in-extensional beam.
15. A. H. NAYFEH and D. T. MOOK 1979 *Nonlinear Oscillations*. New York: Wiley-Interscience.

APPENDIX A

$$h_{11} = \int_0^1 \psi_n^2 \,\mathrm{d}x,$$

$$h_{12} = \int_0^1 \delta(x-\beta)\psi_n^2 \,\mathrm{d}x,$$

$$h_{13} = \int_0^1 \delta(x-\beta)(\psi_{nx})^2 \,\mathrm{d}x = \psi_{nx}^2(\beta),$$

$$h_{21} = \int_0^1 \psi_n^2 \,\mathrm{d}x = h_{11},$$

$$R_n = h_{11} + \mu h_{12} + J\lambda^2 h_{13},$$

$$\zeta_n = \zeta_n^* \nu = \varepsilon\left(\frac{c_{h_{21}}}{2\varepsilon R_n \rho \theta_1}\right)\nu,$$

$$h_{31} = \int_0^1 \psi_n^2 \,\mathrm{d}x,$$

$$h_{32} = \int_0^1 \delta(x-\beta)\psi_i^2 \,\mathrm{d}x = h_{12},$$

$$h_{33} = \int_0^1 (1-x)\psi_{nx}^2 \,\mathrm{d}x,$$

$$h_{34} = \int_0^1 \int_x^1 \delta(\xi-\beta)\,\mathrm{d}\xi \psi_{nx}^2 \,\mathrm{d}x,$$

$$\theta_n^2 = \frac{EI\kappa_n^4}{\rho L^4 R_n}(h_{31} + \mu h_{32}) - \frac{g}{LR_n}(h_{33} + \mu h_{34}),$$

$$f_{nm} = f^{*}_{nm}\Gamma/\varepsilon = \frac{\Omega^2 Z_o}{\varepsilon\theta_1^2 R_n L}(h_{33} + \mu h_{34})$$

$$h_{41} = \frac{1}{2}\int_0^1 \psi_k \psi_{lx} \psi_{mx} \psi_n \, \mathrm{d}x$$

$$h_{42} = \frac{1}{2}\int_0^1 \delta(x-\beta)\psi_k \psi_{lx} \psi_{mx} \psi_n \, \mathrm{d}x$$

$$h_{43} = 3\int_0^1 \psi_{kx}\psi_{lxx}\psi_{mxxx}\psi_n \, \mathrm{d}x + \int_0^1 \psi_{kxx}\psi_{lxx}\psi_{mxx}\psi_n \, \mathrm{d}x$$

$$\alpha^n_{klm} = \frac{EI\lambda^2}{\varepsilon\rho L^4 R_n \theta_1^2}\{\kappa_k^4(h_{41} + \mu h_{42}) + h_{43}\}$$

$$h_{51} = \int_0^1 \left\{\int_x^1 \left(\int_0^\xi \psi_{l_\eta}\psi_{m\eta} \, \mathrm{d}\eta\right) \mathrm{d}\xi\right\}\psi_{kx}\psi_{nx} \, \mathrm{d}x$$

$$h_{52} = \left(\int_0^\beta \psi_{lx}\psi_{mx} \, \mathrm{d}x\right)\left(\int_0^\beta \psi_{kx}\psi_{nx} \, \mathrm{d}x\right)$$

$$h_{53} = \{\psi_{kx}\psi_{lx}\psi_{mx}\psi_{nx}\}_{x=\beta}$$

$$\beta^n_{klm} = \frac{\lambda^2}{\varepsilon R_n}\{h_{51} + \mu h_{52} + J\lambda^2 h_{53}\}$$

$$h_{61} = h_{51}$$

$$h_{62} = \frac{1}{2}\int_0^1 \psi_{kx}\psi_{lx}\psi_m\psi_n \, \mathrm{d}x - \int_0^1 \psi_{kx}\psi_{lxx}\left(\int_x^1 \psi_m \, \mathrm{d}\xi\right)\psi_n \, \mathrm{d}x$$

$$h_{63} = h_{52}$$

$$h_{64} = \frac{1}{2}[\psi_{kx}\psi_{lx}\psi_m\psi_n]_{x=\beta} - \psi_m(\beta)\int_0^\beta \psi_{kx}\psi_{lxx}\psi_n \, \mathrm{d}x$$

$$h_{65} = \frac{1}{2}h_{53}$$

$$\gamma^n_{klm} = \frac{\lambda^2}{\varepsilon R_n}[h_{61} - h_{62} + \mu(h_{63} - h_{64}) + J\lambda^2 h_{65}].$$

Expression for α_{enj}, Q_1, Q_2

$$\alpha_{enj} = \alpha_{nj} + \beta_{nj} + \gamma_{nj},$$

$$\begin{aligned} \alpha_{nj} &= 3\alpha^n_{nnn}, \quad \text{for} \quad j = n \\ &= 2(\alpha^n_{njj} + \alpha^n_{jjn} + \alpha^n_{jnj}), \quad \text{for} \quad j \neq n, \end{aligned}$$

$$
\begin{aligned}
\beta_{nj} &= \omega_n^2 \beta_{nnn}^n, \quad \text{for} \quad j = n, \\
&= 2\omega_j^2 \beta_{njj}^n, \quad \text{for} \quad j \neq n, \\
\gamma_{nj} &= -3\omega_n^2 \gamma_{nnn}^n, \quad \text{for} \quad j = n \\
&= -2\{\omega_j^2(\gamma_{jnj}^n + \gamma_{njj}^n) + \omega_n^2 \gamma_{jjn}^n\}, \quad \text{for} \quad j \neq n, \\
Q_1 &= \alpha_{121}^1 + \alpha_{211}^1 + \alpha_{112}^1 \\
&\quad - \omega_1^2 \beta_{211}^1 + \omega_1 \omega_2 (\beta_{121}^1 + \beta_{112}^1) \\
&\quad - \{\omega_1^2(\gamma_{211}^1 + \gamma_{121}^1) + \omega_2^2 \gamma_{112}^1\}, \\
Q_2 &= \alpha_{111}^2 - \omega_1^2(\beta_{111}^2 + \gamma_{111}^2).
\end{aligned}
$$

The linear undamped mode shape $\psi_n(x)$ can be written in non-dimensional form as

$$
\begin{aligned}
\psi_n(x) = &[(\sin \kappa_n x - \sinh \kappa_n x) - \Lambda(\cos \kappa_n x - \cosh \kappa_n x)] \\
&+ U(x - \beta)\{(h_1 - \Lambda h_2)[\sin \kappa_n(x - \beta) - \sinh \kappa_n(x - \beta)] \\
&+ (h_3 - \Lambda h_4)[\cos \kappa_n(x - \beta) - \cosh \kappa_n(x - \beta)]\},
\end{aligned}
$$

where U is the unit step function and $\psi_n(x)$ is the eigenfunction of the nth mode. The other terms are defined below.

$$
\begin{aligned}
h_1 &= (k_{22} l_{11} - k_{12} l_{12})/D, \\
h_2 &= (k_{22} l_{12} - k_{12} l_{22})/D, \\
h_3 &= (k_{11} l_{12} - k_{12} l_{11})/D, \\
h_4 &= (k_{11} l_{22} - k_{12} l_{12})/D, \\
D &= -2[1 + \cos \kappa_n(1 - \beta) \cosh \kappa_n(1 - \beta)], \\
k_{11} &= \sin \kappa_n(1 - \beta) + \sinh \kappa_n(1 - \beta), \\
k_{12} &= \cos \kappa_n(1 - \beta) + \cosh \kappa_n(1 - \beta), \\
k_{22} &= -\sin \kappa_n(1 - \beta) + \sinh \kappa_n(1 - \beta), \\
l_{11} &= -\sin \kappa_n - \sinh \kappa_n, \\
l_{12} &= -\cos \kappa_n - \cosh \kappa_n,
\end{aligned}
$$

$$
\begin{aligned}
l_{22} &= \sin \kappa_n - \sinh \kappa_n, \\
\Lambda &= [2\mu h_1 + \kappa_n(\sin \kappa_n \beta - \sinh \kappa_n \beta)]/[2\mu h_2 + \kappa_n(\cos \kappa_n \beta - \cosh \kappa_n \beta)].
\end{aligned}
$$

Θ_n is the nth linear natural frequency of the system which is given by

$$\Theta_n^2 = \frac{EI}{\rho}\left(\frac{\kappa_n}{L}\right)^4,$$

κ_n being the eigenvalue of the nth mode of vibration obtained from the solution of the transcendental equation

$$\frac{4(h_1h_4 - h_2h_3)}{\lambda^2\mu J} + 2\kappa^4[1 - \cos\kappa\beta\cosh\kappa\beta]$$
$$+\frac{2\kappa^3}{\mu}[h_1(\sin\kappa\beta + \sinh\kappa\beta) + h_2(\cos\kappa\beta - \cosh\kappa\beta)]$$
$$+\frac{2\kappa}{J\lambda^2}[h_4(\sin\kappa\beta - \sinh\kappa\beta) - h_3(\cos\kappa\beta - \cosh\kappa\beta)] = 0.$$

A.1. PHYSICAL EXAMPLE

A metallic beam is considered with the following properties: $L = 125{\cdot}4$ mm, $I = 0{\cdot}04851$ mm^4, $E = 0{\cdot}20936 \times 10^6$ N/mm^2, $Z_r = 1$ mm, $c = 0{\cdot}1$ N $\cdot$ s/mm^2, $\rho = 0{\cdot}03332$ gm/mm, $\mu = 3{\cdot}68979$, $J = 0{\cdot}959$, $\beta = 0{\cdot}25$. The roots of the characteristic equation are found numerically to be $\kappa_1 = 1{\cdot}80097$, $\kappa_2 = 3{\cdot}2836$ and the corresponding non-dimensional natural frequencies are $\omega_1 = 1$ and $\omega_2 = 3{\cdot}33179$. The book-keeping parameter ε and scaling factor λ are taken as 0·001 and 0·1, respectively. The coefficients of damping (ζ_n), excitation (f_{nm}) and non-linear terms, (α^n_{klm}, β^n_{klm}, γ^n_{klm}) are found to be of the same order. The values of other required parameters expressed in this Appendix are calculated to be: $\alpha_{e11} = 2{\cdot}54149$, $\alpha_{e12} = -12{\cdot}2027$, $\alpha_{e21} = -6{\cdot}63699$, $\alpha_{e22} = -195{\cdot}55$, $Q_1 = 14{\cdot}62282$, $Q_2 = 7{\cdot}84674$, $f^*_{11} = 0{\cdot}0655762$, $f^*_{12} = 0{\cdot}0122118$, $f^*_{21} = 0{\cdot}04249$, $f^*_{22} = 0{\cdot}1699298$, $\zeta^*_1 = 0{\cdot}0118963$, $\zeta^*_2 = 0{\cdot}0045865$.

APPENDIX B: NOTATION

u_n	lateral displacement of the nth mode of beam vibration
L	length of the beam
E	Young's modulus of the beam
I	moment of inertia of the beam section
J_o	polar moment of inertia of the attached mass
J	non-dimensional polar moment of inertia of the attached mass $= J_o/\rho L r^2$
r	scaling factor used in multi-mode discretization
m	mass of the attached element
ρ	mass per unit length of the beam
d	length of the attached element from the base (Figure 1)
s	reference variable along beam (Figure 1)
x	$= s/L$

c	coefficient of damping
z	vertical base excitation ($=Z_o \cos \Omega t$)
μ	mass ratio (mass of attached element/mass of the beam)
β	location parameter ($=d/L$)
ζ_n	damping ratio of the nth mode
θ_n	natural frequency of nth mode (dimensional)
ω_n	natural frequency of the nth mode (non-dimensional)
ϕ	non-dimensional frequency of external excitation ($=\Omega/\theta_1$)
f_{nm}	forcing parameter in the nth mode due to interaction of the mth mode
α^n_{klm}	geometric non-linearities
β^n_{klm}	inertial non-linearities
γ^n_{klm}	inertial non-linearities
Γ	non-dimensional amplitude of external excitation ($=Z_o/Z_r$)
ν	damping parameter ($=\zeta_n/\zeta^*_n$)
Z_r	scaling parameter
t	time
τ	non-dimensional time ($=\theta_1 t$)
ε	book-keeping parameter to indicate smallness of damping, non-linearities and forcing parameter
σ_1, σ_2	external and internal detuning parameters
a_n	amplitude of excitation of the nth mode
γ_n	phase of excitation of the nth mode